

# Model Predictive Direct Torque Control: Derivation and Analysis of the State-Feedback Control Law

Tobias Geyer, *Senior Member, IEEE*

**Abstract**—This paper derives and visualizes the explicit state-feedback control law of model predictive controllers for electrical drives, using model predictive direct torque control as an illustrative example. The control law is given over the whole state-space and computed in an offline procedure. The availability of the control law allows one to analyze the controller, and to visualize and better understand its behavior and decision making process. Based on this concept, numerous other important tasks can be accomplished, such as stability analysis, feasibility analysis, reduction of the computational effort, derivation of switching heuristics and the further improvement of the closed-loop performance.

**Index Terms**—Model predictive direct torque control, model predictive control, state-feedback control law, variable-speed drives, medium-voltage drives

## NOTATION

$\varphi$	Angle between the $a$ -axis of the three-phase system and the $d$ -axis of the reference frame.
$\theta$	Load angle, i.e. angle between the stator and rotor flux vectors.
$\psi_s$	Stator flux vector with $\psi_s = [\psi_{sd} \ \psi_{sq}]^T$ .
$\psi_r$	Rotor flux vector with $\psi_r = [\psi_{rd} \ \psi_{rq}]^T$ .
$\Psi_s$	Magnitude of the stator flux vector $\ \psi_s\ $ .
$\Psi_r$	Magnitude of the rotor flux vector $\ \psi_r\ $ .
$T_e$	Electromagnetic torque.
$T_{e,\text{ref}}$	Reference value of the electromagnetic torque.
$T_{e,\text{min}}$	Lower bound on the electromagnetic torque.
$T_{e,\text{max}}$	Upper bound on the electromagnetic torque.
$J$	Cost function.
$N_p$	Length of the prediction horizon (number of time-steps).
$\epsilon_y$	Rms bound violation of the torque and stator flux magnitude with $\epsilon_y = [\epsilon_T \ \epsilon_\Psi]^T$ .
$q$	Penalty weight on bound violations.
$\mathbf{u}$	Control input (three-phase switch position).
$\mathbf{u}^*$	Optimal control input.
$\mathbf{v}_s$	Stator voltage.
$\mathbf{x}$	State vector with $\mathbf{x} = [\psi_{s\alpha} \ \psi_{s\beta} \ \psi_{r\alpha} \ \psi_{r\beta}]^T$ .
$\omega_{\text{fr}}$	Angular speed of the $dq$ reference frame.
$\omega_r$	Electrical angular speed of the rotor.

## I. INTRODUCTION

Model predictive direct torque control (MPDTC) is an emerging control concept for three-phase electrical drive

system [1]–[4], adopting the principles of model predictive control (MPC) [5], [6]. MPDTC is particularly well suited for medium-voltage drives, which are based on multi-level voltage source inverters and operate at very low switching frequencies [7]. Compared with state-of-the-art schemes, such as direct torque control (DTC) [8] and field oriented control (FOC) [9] with space vector modulation (SVM), MPDTC achieves a reduction of the switching losses by up to 50% [4] for three-level neutral point clamped inverters. Alternatively, the current or torque distortions can be reduced by the same amount [10]. For five-level topologies, the performance benefits are even more pronounced, as shown in [11] and [12].

Unlike DTC or FOC with SVM, MPDTC is based on an online optimization stage. Given the torque and stator flux references and their estimated values, a suitable inverter switch position is computed, minimizing the switching effort (either the switching frequency or the switching losses). This optimization is based on an internal model of the drive that enables the controller to predict the impact the switching transitions under consideration have on the torque, currents and flux vectors. Unlike in DTC, the control law is not directly available—for example in form of a look-up table—and thus cannot be analyzed easily and visualized, complicating the design process and the understanding of MPDTC.

This issue motivates this paper. The state-feedback control law, which is the control input (the switch position) represented as a function of the state vector over the state-space, is computed, visualized and analyzed. The impact of varying the length of the switching horizon will be shown. The information and insight obtained is not only meant to further the understanding of MPDTC, but it is also envisioned that this will help revise and improve the MPDTC algorithm, e.g. with the aim to lower its computational burden. The techniques proposed in this paper are directly applicable to other predictive drive control methods, including one-step predictive control [13].

When formulating MPC problems for linear and piecewise affine (linear plus offset) systems with piecewise affine constraints, so called hybrid systems, the explicit solutions can be computed in a mathematically elegant way. The resulting control input is piecewise affine in the state vector. Specifically, the state space is divided into polyhedral regions and the control input for each region is affine in the state vector, i.e. linear plus an offset. For more details on the explicit solution of MPC for piecewise affine systems, the reader is referred to [14] and the references therein. The multi-parametric toolbox provides a powerful set of tools to compute and analyze such

T. Geyer is now with ABB Corporate Research, 5405 Baden-Dättwil, Switzerland (e-mail: t.geyer@ieee.org). This work was done at the Department of Electrical and Computer Engineering, The University of Auckland, Auckland, New Zealand.

solutions [15].

For three-phase electrical drive systems we have previously derived explicit control laws, by approximating the nonlinearities of the torque and stator flux magnitude by piecewise affine functions, modelling the drive system in the mixed logical dynamical (MLD) framework [16], formulating the MPC control problem as a closed-form optimization problem and using a modified version of the MPT toolbox to derive the explicit control law. Due to the daunting computational complexity, this approach was only applicable to two-level inverters [1], [17] and dc-dc converters [18]. A problem specific computational scheme, which exploits the structure of the drive control problem, was proposed in [19]. An explicit solution for a simplified FOC problem was described in [20]. In this paper, however, we refrain from approximating the drive model and formulate the control problem as an open-form optimization problem. As a result, the standard techniques from hybrid control theory to compute explicit solutions are not applicable.

The paper is organized as follows. After describing the drive system case study in the next section, the model predictive control problem is formally stated in Sect. III. The MPDTC solution approach and algorithm is summarized in Sect. IV. The control law for MPDTC is computed, visualized and analyzed in detail in Sects. V and VI. Section VII provides concluding remarks.

## II. DRIVE SYSTEM CASE STUDY

Throughout this paper, we will use normalized quantities. Extending this to the time scale  $t$ , one time unit corresponds to  $1/\omega_b$  seconds, where  $\omega_b$  is the base angular velocity. Additionally, we will use  $\xi(t)$ ,  $t \in \mathbb{R}$ , to denote continuous-time variables, and  $\xi(k)$ ,  $k \in \mathbb{N}$ , to denote discrete-time variables with the sampling interval  $T_s = 25 \mu\text{s}$ .

### A. Reference Frames

All variables  $\xi_{abc} = [\xi_a \ \xi_b \ \xi_c]^T$  in the three-phase system ( $abc$ ) can be transformed to  $\xi_{dq0} = [\xi_d \ \xi_q \ \xi_0]^T$  in the orthogonal rotating  $dq0$  reference frame through  $\xi_{dq0} = \mathbf{P}(\varphi) \xi_{abc}$ , where  $\varphi$  denotes the angle between the  $a$ -axis of the three-phase system and the  $d$ -axis of the reference frame. By aligning the  $d$ -axis with the motor's rotor flux,  $\varphi$  also corresponds to the rotor's angular position, see Fig. 2. The transformation matrix is given by

$$\mathbf{P}(\varphi) = \frac{2}{3} \begin{bmatrix} \cos(\varphi) & \cos(\varphi - \frac{2\pi}{3}) & \cos(\varphi + \frac{2\pi}{3}) \\ -\sin(\varphi) & -\sin(\varphi - \frac{2\pi}{3}) & -\sin(\varphi + \frac{2\pi}{3}) \\ \frac{1}{2} & \frac{1}{2} & \frac{1}{2} \end{bmatrix}. \quad (1)$$

The reference frame rotates with the angular speed  $\omega_{fr} = d\varphi/dt$ .

The stationary (i.e. non-rotating)  $\alpha\beta0$  reference frame is obtained by setting both  $\varphi$  and  $\omega_{fr}$  to zero. The  $d$ - and  $q$ -axes are then referred to as  $\alpha$ - and  $\beta$ -axes, respectively, with the 0-axis remaining unchanged. The transformation from the  $abc$  to the  $\alpha\beta0$  reference frame is defined through  $\xi_{\alpha\beta0} = \mathbf{P}(0)\xi_{abc}$ .

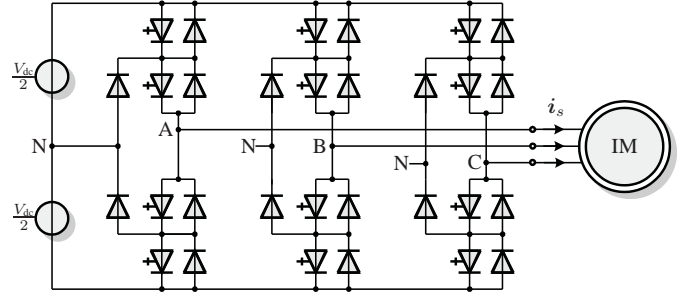


Fig. 1: Three-level neutral point clamped voltage source inverter driving an induction motor with a fixed neutral point potential

### B. NPC Inverter

As an example for a medium-voltage drive system, consider a three-level neutral point clamped (NPC) voltage source inverter with an induction machine, as shown in Fig. 1. The inverter is fed by two constant dc-link voltage sources, and its total dc-link voltage is  $V_{dc} = 5.2 \text{ kV}$ . ABB's 35L4510 4.5 kV 4 kA IGCT and ABB's 10H4520 fast recovery diode are used as semiconductor devices.

Let the integer variables  $u_a, u_b, u_c \in \{-1, 0, 1\}$  denote the switch positions in each phase leg, where the values  $-1, 0, 1$  correspond to the phase voltages  $-\frac{V_{dc}}{2}, 0, \frac{V_{dc}}{2}$ , respectively. The actual voltage applied to the machine terminals is given by  $v_{s,\alpha\beta0} = 0.5V_{dc} \mathbf{P}(0) \mathbf{u}_{abc}$  with  $\mathbf{u} = \mathbf{u}_{abc} = [u_a \ u_b \ u_c]^T$ . Direct switching between the upper and lower rails is prohibited, i.e.  $\|\Delta \mathbf{u}(k)\|_\infty \leq 1$  is imposed with  $\Delta \mathbf{u}(k) = \mathbf{u}(k) - \mathbf{u}(k-1)$ .

Switching losses arise in the inverter when turning the semiconductors on or off and commutating the phase current. These losses depend on the applied voltage, the commutated current and the semiconductor characteristics. For Integrated Gate Commutated Thyristors (IGCT), with the GCT being the semiconductor switch, the turn-on and turn-off losses can be well approximated to be linear in the dc-link voltage and the phase current. Yet for diodes, the reverse recovery losses are linear in the voltage, but nonlinear in the commutated current.

As shown in [4], [21], the switching losses can be derived as a function of the switching transition, the commutated phase current and its polarity. The turn-on (energy) loss of a GCT, for example, is given by

$$E_{on} = e_{on} \frac{1}{2} V_{dc} i_{ph}, \quad (2)$$

where  $e_{on}$  is a GCT specific coefficient, which is readily available from the manufacturer's data sheets, and  $i_{ph}$  is the phase current. For the GCT turn-off and diode reverse recovery losses, similar equations can be derived.

### C. Induction Machine

The machine considered here is a 3.3 kV and 50 Hz squirrel-cage induction machine rated at 2 MVA. A summary of the machine parameters can be found in Table I. The induction machine is modeled in the  $\alpha\beta$  reference frame using the  $\alpha$ - and  $\beta$ -components of the stator and rotor flux linkages per

second,  $\psi_{s\alpha}$ ,  $\psi_{s\beta}$ ,  $\psi_{r\alpha}$  and  $\psi_{r\beta}$ , respectively, as state variables. The rotor speed dynamic is neglected and the rotor's angular speed  $\omega_r$  is assumed to remain constant within the prediction horizon.

The model parameters are the stator and rotor resistances  $R_s$  and  $R_r$ , and the stator, rotor and mutual reactances  $X_{ls}$ ,  $X_{lr}$  and  $X_m$ , respectively. Introducing  $\psi_s = [\psi_{s\alpha} \ \psi_{s\beta}]^T$  and accordingly  $\psi_r$  and  $v_s$ , the state equations of the machine can be written as [22]

$$\frac{d\psi_s}{dt} = -R_s \frac{X_r}{D} \psi_s + R_s \frac{X_m}{D} \psi_r + v_s \quad (3a)$$

$$\frac{d\psi_r}{dt} = R_r \frac{X_m}{D} \psi_s - R_r \frac{X_s}{D} \psi_r + \omega_r \begin{bmatrix} 0 & -1 \\ 1 & 0 \end{bmatrix} \psi_r \quad (3b)$$

with  $X_s = X_{ls} + X_m$ ,  $X_r = X_{lr} + X_m$  and  $D = X_s X_r - X_m^2$ .

The electromagnetic torque is given by

$$T_e = \frac{X_m}{D} \psi_r \times \psi_s = \sin(\theta) \Psi_s \Psi_r, \quad (4)$$

with the load angle  $\theta$ , which is the angle between the stator and rotor flux vectors. Moreover,  $\Psi_s = \|\psi_s\|$  and  $\Psi_r = \|\psi_r\|$  denote the length of the stator and rotor flux vector, respectively. For more details on the modelling of the induction machine, the reader is referred to [1], [2], [4] and [22].

### III. MPC PROBLEM FORMULATION

#### A. Control Problem

The control problem is to keep the machine's torque and stator flux magnitude within given bounds around their respective references. During transients, a high dynamic performance is to be ensured, i.e. a short torque settling time in the range of a few ms. Under steady state operating conditions, the total harmonic distortion (THD) of the current is to be kept small, so as to reduce the copper losses and thus the thermal losses in the stator windings of the machine. In addition, to avoid problems with the mechanical load, such as wear of the shaft and the possible excitation of eigenfrequencies of the load, the torque THD needs to be kept at a minimum.

Regarding the inverter, the switching losses in the semiconductors are to be minimized. An indirect way of achieving this is to reduce the device switching frequency.

#### B. Target Window

Let  $T_{e,\text{ref}}$  denote the reference of the electromagnetic torque. The upper and lower torque bounds are given by  $T_{e,\text{max}}$  and  $T_{e,\text{min}}$ , respectively. The reference of and bounds on the

Induction machine	Voltage	3300 V	$R_s$	0.0108 pu
	Current	356 A	$R_r$	0.0091 pu
	Real power	1.587 MW	$X_{ls}$	0.1493 pu
	Apparent power	2.035 MVA	$X_{lr}$	0.1104 pu
	Frequency	50 Hz	$X_m$	2.3489 pu
	Rotational speed	596 rpm		
Inverter			$V_{dc}$	1.930 pu

TABLE I: Rated values (left) and parameters (right) of the drive

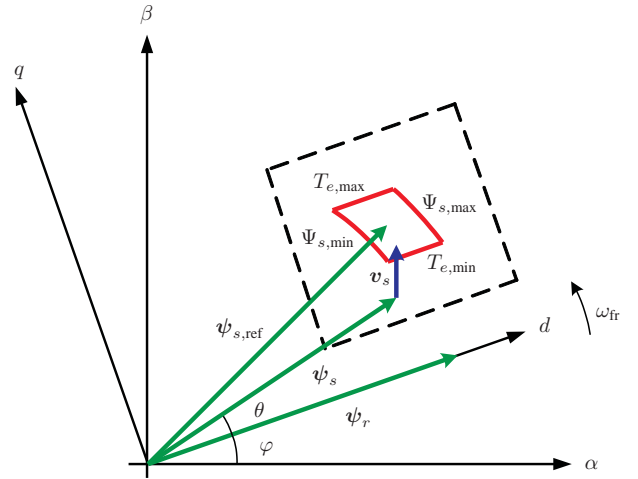


Fig. 2: Stator and rotor flux vectors  $\psi_s$  and  $\psi_r$  in the  $dq$ -reference frame, which rotates with the angular velocity  $\omega_{fr}$ . The target window around the stator flux reference  $\psi_{s,\text{ref}}$  is indicated by straight (red) lines, which correspond to the upper and lower bounds on the torque and stator flux magnitude, respectively. The stator flux vector is driven by the voltage vector  $v_s$ . The dashed (black) lines indicate the rectangular set for which the state-feedback control law will be derived

magnitude of the stator flux vector are defined accordingly as  $\Psi_{s,\text{ref}}$ ,  $\Psi_{s,\text{max}}$  and  $\Psi_{s,\text{min}}$ .

For a given rotor flux vector  $\psi_r$ , the references on the torque and stator flux magnitude can be translated into an equivalent reference stator flux vector  $\psi_{s,\text{ref}}$ , as shown in Fig. 2. The upper and lower torque and flux magnitude bounds can be translated accordingly into the stator flux space, spanned by its  $d$ - and  $q$ -components. These bounds are thus equivalent to a *target window* in the space of the stator flux vector. Keeping the stator flux vector within this window is equivalent to maintaining the electromagnetic torque and the stator flux magnitude within their upper and lower bounds, thus ensuring that the desired electromagnetic torque is generated and that the machine is appropriately magnetized.

Under steady-state operating conditions, the target window rotates in synchronism with the rotor flux vector. Specifically, the target window is stationary within the  $dq$  reference frame, with the torque bounds being parallel to the  $d$ -axis, while the flux bounds are ring segments around the origin. During transients, such as torque steps, the target window is shifted along the  $q$ -axis. In this case, violations of the target window might occur, and the stator flux vector is to be moved back into the target window as quickly as possible, so as to ensure a minimal torque settling time and to avoid too high or too low a stator flux magnitude.

#### C. Model Predictive Control Principle

The drive control problem can be addressed by adopting the notion of model predictive control (MPC) [6]. Specifically, a discrete-time model of the drive system is used to predict the machine's response and the switching effort as a function of possible switching sequences over a long prediction horizon. At each time-step, the controller computes a sequence of

switch positions over the prediction horizon that keeps the torque and stator flux magnitude within the imposed bounds and minimizes the switching frequency or losses. Out of this sequence, only the first gating signal is applied to the inverter, and the optimization step is repeated with new measurements at the next sampling instant. Typically, the sampling interval is with  $T_s = 25 \mu\text{s}$  very short, while the prediction horizon entails up to 160 steps and is thus up to 4 ms long [4].

#### D. Optimization Problem

Writing the above control problem as a closed-form optimization problem leads to

$$J^*(\mathbf{x}(k), \mathbf{u}(k-1)) = \min_{\mathbf{U}(k)} (J_{\text{sw}} + J_{\text{bnd}}) \quad (5a)$$

$$\text{s. t. } \mathbf{x}(\ell+1) = \mathbf{A}\mathbf{x}(\ell) + \mathbf{B}\mathbf{u}(\ell) \quad (5b)$$

$$\mathbf{y}(\ell+1) = \mathbf{g}(\mathbf{x}(\ell+1)) \quad (5c)$$

$$\mathbf{y}(\ell+1) \in \mathcal{Y} \text{ or } \varepsilon_y(\ell+1) < \varepsilon_y(\ell) \quad (5d)$$

$$\mathbf{u}(\ell) \in \mathcal{U}, \quad \|\Delta\mathbf{u}(\ell)\|_\infty \leq 1 \quad (5e)$$

$$\forall \ell = k, \dots, k + N_p - 1, \quad (5f)$$

with  $J^*$  denoting the minimum of the objective function  $J = J_{\text{sw}} + J_{\text{bnd}}$ . The latter is a function of the state vector  $\mathbf{x} = [\psi_{s\alpha} \ \psi_{s\beta} \ \psi_{r\alpha} \ \psi_{r\beta}]^T$  at the current time-instant  $k$  and the switch position  $\mathbf{u}(k-1)$ , which was set in the previous control cycle. The sequence of control inputs  $\mathbf{U}(k) = [\mathbf{u}^T(k), \mathbf{u}^T(k+1), \dots, \mathbf{u}^T(k+N_p-1)]^T$  over the prediction horizon  $N_p$  represents the sequence of inverter switch positions the controller decides upon. The objective function (5a) is minimized for all  $\mathbf{U}(k)$  subject to the dynamical evolution of the machine (5b), its outputs (5c) and the constraints (5d) and (5e). The variables in (5) are defined in the remainder of this section.

#### E. Objective Function

The objective function consists of two parts: The first part  $J_{\text{sw}}$  captures the switching effort. Specifically,

$$J_f = \frac{1}{N_p} \sum_{\ell=k}^{k+N_p-1} \|\Delta\mathbf{u}(\ell)\|_1 \quad (6)$$

represents the sum of the switching transitions (number of commutations) over the prediction horizon divided by the length of the horizon—it thus approximates the short-term switching *frequency*. Alternatively, the switching (power) *losses* can be directly represented through

$$J_P = \frac{1}{N_p} \sum_{\ell=k}^{k+N_p-1} E_{\text{sw}}(\mathbf{x}(\ell), \mathbf{u}(\ell), \mathbf{u}(\ell-1)), \quad (7)$$

which is the sum of the instantaneous switching (energy) losses  $E_{\text{sw}}$  over the prediction horizon. Note that, according to (2),  $E_{\text{sw}}$  is a function of the stator current  $i_s$ , which in turn depends linearly on the state vector  $\mathbf{x}$ . In (5a) we either use  $J_{\text{sw}} = J_f$  or  $J_{\text{sw}} = J_P$ .

The drive's output vector  $\mathbf{y} = [T_e \ \Psi_s]^T$  represents the electromagnetic torque and the stator flux magnitude. To

quantify the degree of a bound violation, we introduce for the torque

$$\varepsilon_T = \begin{cases} T_e - T_{e,\text{max}} & \text{if } T_e \geq T_{e,\text{max}} \\ T_{e,\text{min}} - T_e & \text{if } T_e \leq T_{e,\text{min}} \\ 0 & \text{else.} \end{cases} \quad (8)$$

The rms bound violation of the torque over the prediction horizon can be captured by

$$\varepsilon_T(k) = \sqrt{\frac{1}{N_p} \sum_{\ell=k}^{k+N_p-1} (\varepsilon_T(\ell))^2}. \quad (9)$$

For the stator flux magnitude,  $\varepsilon_\Psi$  and  $\varepsilon_y$  are defined accordingly. The second term in the objective function (5a),

$$J_{\text{bnd}} = q \varepsilon_y^T \varepsilon_y, \quad (10)$$

penalizes the rms bound violation of the output vector, which is  $\varepsilon_y = [\varepsilon_T \ \varepsilon_\Psi]^T$ . The parameter  $q$  is a positive scalar weighting term.

#### F. Internal Prediction Model

The internal prediction model is derived by rewriting the continuous-time machine equations (3) in the state-space form  $\frac{d\mathbf{x}}{dt}(t) = \mathbf{F}\mathbf{x}(t) + \mathbf{G}\mathbf{u}(t)$ . The exact Euler discretization method is used to derive the discrete-time matrices

$$\mathbf{A} = e^{\mathbf{F}T_s} \text{ and } \mathbf{B} = -\mathbf{F}^{-1}(\mathbf{I} - \mathbf{A})\mathbf{G} \quad (11)$$

for the discrete-time state-space representation of the machine model (5b), with  $e$  denoting the matrix exponential,  $T_s$  the sampling interval and  $\mathbf{I}$  the identity matrix. As mentioned earlier, the motor speed is assumed to be constant within the prediction horizon—the speed is thus not part of the state vector but rather a parameter of the model (5b).

#### G. Constraints

The lower and upper bounds on the torque and stator flux magnitude form the set  $\mathcal{Y} = [T_{e,\text{min}}, T_{e,\text{max}}] \times [\Psi_{s,\text{min}}, \Psi_{s,\text{max}}]$ . The constraint (5d) is imposed componentwise, i.e. separately for the torque and the stator flux magnitude. If at time-step  $k$  an output variable is within its bounds, then it has to stay within them. This is the standard case during steady-state operation. If, however, at time-step  $k$  a variable violates a bound, then it has to move closer to the bound at every time-step  $\ell$  within the prediction horizon, where  $\ell = k, \dots, k + N_p - 1$ .

The constraint (5e) limits the control input  $\mathbf{u}$  to the integer values  $\mathcal{U} = \{-1, 0, 1\}^3$  available for the three-level inverter. Switching in a phase by more than one step up or down is not allowed. This is enforced by the second constraint in (5e),  $\|\Delta\mathbf{u}(\ell)\|_\infty \leq 1$ , which limits the elements in  $\Delta\mathbf{u}$  to  $\pm 1$ . These constraints have to be met at every time-step  $\ell$  within the prediction horizon.

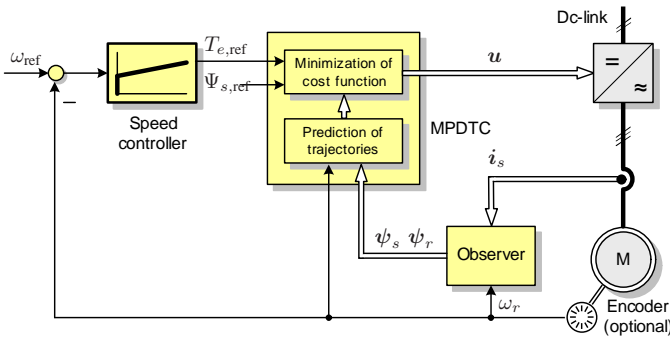


Fig. 3: Model predictive direct torque control (MPDTC) for a voltage source inverter driving an electrical machine

## IV. MODEL PREDICTIVE DIRECT TORQUE CONTROL

### A. MPDTC Solution Approach

The above optimization problem can be solved in real-time by a tailored approach that relies on the fact that switching is mainly required in the vicinity of the bounds or when bounds have been violated. When the torque and stator flux magnitude are well within their bounds, switching is not required and the switch position is frozen.

This gives rise to two different prediction horizons—the switching horizon (the number of switching instants within the horizon, i.e. the controller’s degree of freedom) and the prediction horizon (the number of time-steps MPDTC looks into the future). Between the switching instants the switch positions are frozen and the drive behavior is extrapolated until a bound is hit. The concept of extrapolation leads to long prediction horizons (typically 100 time-steps), while the switching horizon is very short (usually one to three). The switching horizon is composed of the elements ‘S’ and ‘E’, which stand for ‘switch’ and ‘extrapolate’ (or more generally ‘extend’), respectively. We use the task ‘e’ to add an optional extension leg to the switching horizon. For more details about the concept of the switching horizon, refer to [4].

### B. MPDTC Algorithm

The drive’s system state is fully described by the pair  $\mathbf{x}(k)$  and  $\mathbf{u}(k-1)$ , i.e. the machine state and the previously chosen inverter switch position. Based on those, the optimal control input  $\mathbf{u}^*(k)$  can be computed according to the following procedure.

- 1) Initialize the root node with the current state vector  $\mathbf{x}(k)$ , the switch position  $\mathbf{u}(k-1)$  and the switching horizon. Push the root node onto the stack.
- 2a) Take the top node with a non-empty switching horizon from the stack.
- 2b) Read out the first element. For ‘S’, branch on all feasible switching transitions, according to (5e). Use the internal prediction model (5b) to compute the state vector at the next time-step. For ‘E’, extend the trajectories either by using extrapolation, as detailed in [1], [2], or by using extrapolation with interpolation, as proposed in [23].
- 2c) Keep only the switching sequences that meet (5d).

- 2d) Push these sequences onto the stack.
- 2e) Stop if there are no more nodes with non-empty switching horizons. The result of this are the switching sequences  $\mathbf{U}^i(k)$  over the variable-length prediction horizons  $N_p^i$ , where  $i \in \mathcal{I}$  and  $\mathcal{I}$  is an index set.
- 3) Compute for each sequence  $i \in \mathcal{I}$  the associated cost  $J_i$ , as defined in (5a).
- 4) Choose the switching sequence  $\mathbf{U}^* = \mathbf{U}^i(k)$  with the minimal cost, where  $i = \arg \min_{i \in \mathcal{I}} J_i$ .
- 5) Apply (only) the first switch position  $\mathbf{u}^*(k)$  out of this sequence and execute the above procedure again at the next time-step  $k+1$ .

For an in-depth description and analysis of this algorithm, the reader is referred to [2] and [4]. It is straightforward to consider the balancing of a neutral point potential, see e.g. [2], [4], and of other internal voltages of the inverter, as shown in [12]. Branch and bound techniques can be used to reduce the computation time by an order of magnitude [24]. Smart extrapolation methods can be used to increase the accuracy of the predictions [23]. Infeasible states, so called deadlocks, can be largely avoided, by adding terminal weights and terminal constraints [25] to (5). A deadlock resolution strategy has been proposed in [3].

As shown in Fig. 3, MPDTC constitutes an inner torque and flux control loop, which is typically augmented by an outer speed control loop. Depending on the operating point (speed and torque) the torque and stator flux bounds are adjusted by an external loop so as to maintain an acceptable switching frequency.

### V. CONTROL LAW FOR A GIVEN ROTOR FLUX VECTOR

The state-feedback control law is the optimal control input  $\mathbf{u}^*$  represented as a function of the state vector  $\mathbf{x}$  over the state-space  $\mathcal{X}$  of interest, i.e.

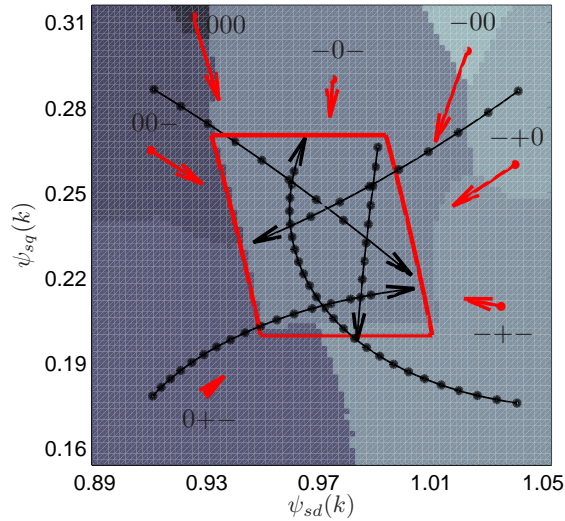
$$\mathbf{u}^*(k) = \mathbf{f}_{\text{MPC}}(\mathbf{x}(k)), \quad \mathbf{x} \in \mathcal{X}. \quad (12)$$

The function  $\mathbf{f}_{\text{MPC}}$  can be evaluated by executing the MPDTC algorithm summarized in the previous section. In a closed-loop drive control setting, these computations are performed online and in real-time. The control law is not directly available. This section proposes a technique to compute offline the control law.

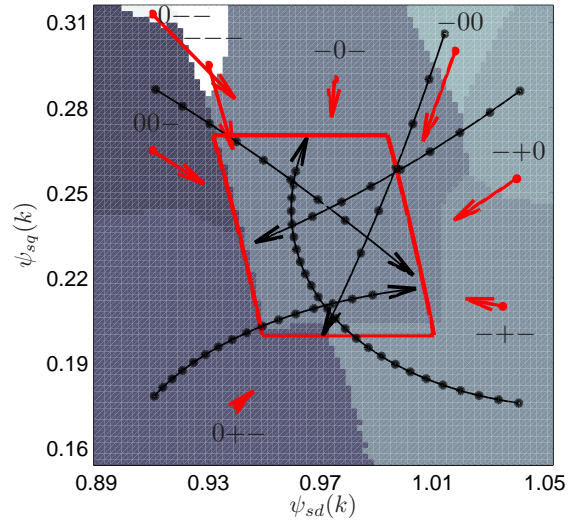
#### A. Assumptions and Settings

In the sequel, the per unit (pu) system is adopted. The pu system is established using the base quantities  $V_B = \sqrt{2/3}V_{\text{rat}} = 2694 \text{ V}$ ,  $I_B = \sqrt{2}I_{\text{rat}} = 503.5 \text{ A}$  and  $f_B = f_{\text{rat}} = 50 \text{ Hz}$ . To simplify the notation, if not otherwise stated, we will drop the pu symbol from all variables and parameters, including the speed, torque, stator and rotor fluxes, and the corresponding upper and lower bounds.

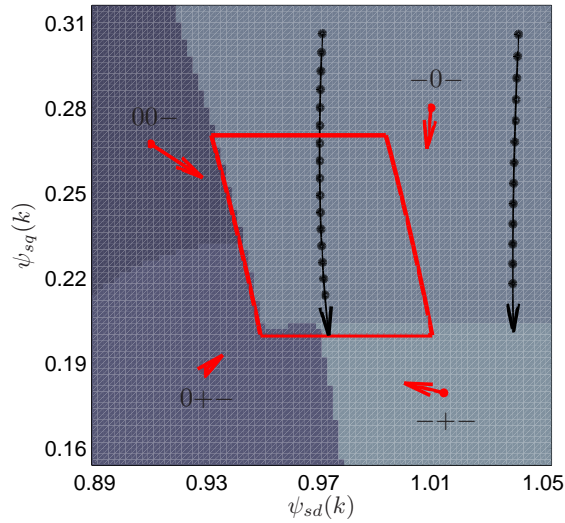
In general, not the whole four-dimensional state-space is of interest. Assume that the machine operates with a constant rotor flux magnitude. This reduces the dimension of the state-space from four to three, with the remaining state variables being the stator flux vector in  $d$  and  $q$ , and the angular position



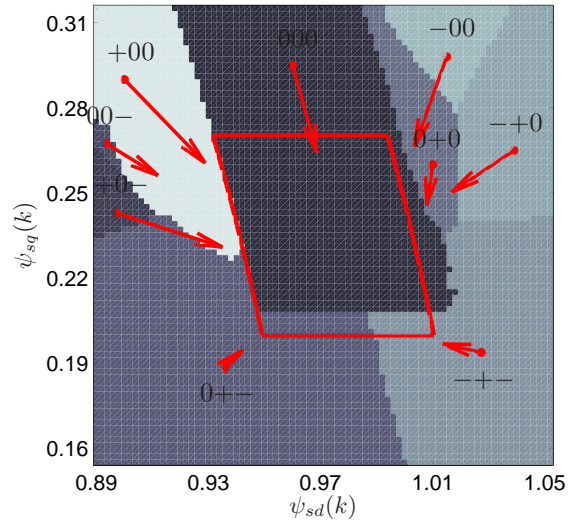
(a) When minimizing the switching losses



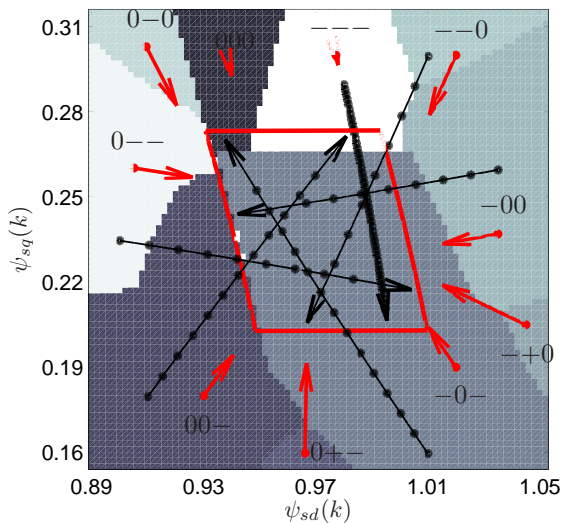
(b) When minimizing the switching frequency



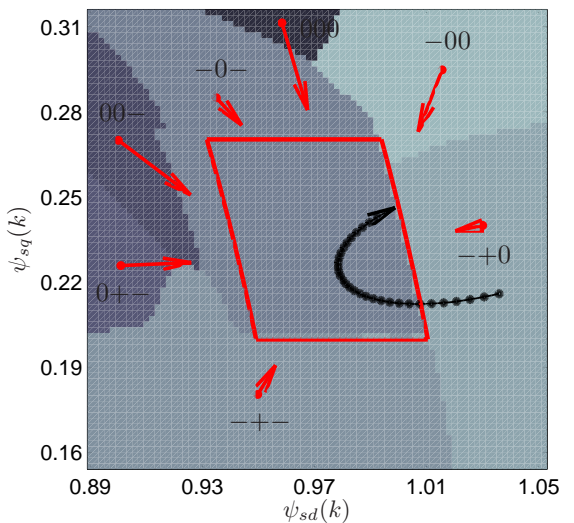
(c) For  $q = 0$



(d) For  $\mathbf{u}(k-1) = [0 \ 0 \ 0]^T$



(e) For  $\omega_r = 0.1$



(f) For  $\varphi(k) = 30^\circ$

Fig. 4: State-feedback control laws, i.e. inverter switch position  $\mathbf{u}^*(k)$  as a function of the state vector  $\mathbf{x}(k)$ , for the inverter switch position  $\mathbf{u}(k-1)$  and the rotor flux angle  $\varphi(k)$ . Predicted stator flux trajectories are shown as black lines, while the target window is indicated by straight (red) lines. The (red) arrows indicate the voltage vectors. If not otherwise stated, the rotor flux angle is  $\varphi(k) = 0^\circ$ , the speed operating point is  $\omega_r = 1$ , and the current switch position is  $\mathbf{u}(k-1) = [-1 \ 0 \ -1]^T$ . In all cases, the switching horizon 'SE' is used

of the rotor flux vector  $\varphi$ . We also assume, without loss of generality, that the machine operates at a constant speed. This implies that the  $dq$  frame rotates with a constant angular velocity.

The operating point is at nominal speed and torque, i.e.  $\omega_r = 1$  and  $T_{e,\text{ref}} = 1$ . For the machine with the parameters given in Table I, at steady-state, the magnitude of the rotor flux vector is  $\|\psi_r\| = 0.92$  and the stator flux reference vector in  $dq$  is  $\psi_{s,\text{ref}} = [0.972 \ 0.235]^T$ . The bounds on the electromagnetic torque are chosen as  $T_{e,\text{min}} = 0.85$  and  $T_{e,\text{max}} = 1.15$ , whereas the bounds on the stator flux magnitude are  $\Psi_{s,\text{min}} = 0.97$  and  $\Psi_{s,\text{max}} = 1.03$ . This defines the target window around  $\psi_{s,\text{ref}}$ .

Consider the switching horizon 'SE'<sup>1</sup> and the objective function  $J = J_P + J_{\text{bnd}}$ , see (5a), (7) and (10), which targets the switching losses. The penalty on the bound violation is set to  $q = 2$ , see (10). The control law is derived for stator flux vectors within the dashed rectangle in Fig. 2 and for the rotor flux angle  $\varphi(k) = 0^\circ$ . The dashed rectangle is centered around the stator flux reference vector, its edges are parallel to the  $d$ - and  $q$ -axes, and the length of its edges is chosen to be 0.16 pu. The edge length along with the rotor flux angle  $\varphi(k)$  defined above determines the subset  $\mathcal{X}$  of the state-space, in which the control law is to be computed.

### B. Algorithm

In order to compute the control law, the stator flux vector is varied within the dashed rectangle shown in Fig. 2. Specifically, a fine grid is generated along the  $d$ - and  $q$ -axes that corresponds to stator flux positions within the rectangle. These grid points, along with  $\varphi$  and  $\|\psi_r\|$  fully define the machine's state vector  $\mathbf{x}$ . Then, for a given switch position  $\mathbf{u}(k-1)$ , the optimal control input  $\mathbf{u}^*(k)$  can be computed for each grid point, yielding the state-feedback control law. The latter can be stored in a table.

### C. State-Feedback Control Law

Several control laws, which resulted from this procedure, are shown in Fig. 4. The optimal switch positions  $\mathbf{u}^*(k)$  are plotted in the two-dimensional state-space, spanned by  $\psi_s$ . Different shades of grey refer to different switch positions. As can be seen, neighboring state vectors (grid points) refer to the same switch position, forming distinctive regions in the state-space, which share the same control input. The switch positions of these regions are indicated using the notation +, 0 and -. For example, 00- refers to  $\mathbf{u}^*(k) = [0 \ 0 \ -1]^T$ .

The target window is shown as the slightly curved parallelogram with straight (red) lines. The (red) arrows correspond to the voltage vectors in  $dq$ . The length of these arrows indicates the amount by which the stator flux vector is moved within 100  $\mu\text{s}$ . This highlights the different velocities by which and the directions in which the different switch combinations drive the stator flux vector relative to the rotating  $dq$  reference frame.

<sup>1</sup>Recall that 'SE' implies that switching is considered only at time-step  $k$ . From time-step  $k+1$  onwards, the switch position is frozen and the output trajectories are extended or extrapolated until a bound is hit.

Moreover, selected predicted stator flux trajectories, which correspond to the respective control input, are shown for several regions. Every second sampling instant (i.e. every 50  $\mu\text{s}$ ) along the trajectories is indicated by a small circle. These trajectories start at selected stator flux vectors and terminate when a bound is about to get violated, thus predicting that switching will be required at this point in the future. The length of the trajectories corresponds to the prediction horizon  $N_p$ . In Fig. 4(a) for example, for the stator flux trajectory starting in the lower right region with  $\mathbf{u}^*(k) = [-1 \ 1 \ -1]^T$ , the prediction horizon is  $N_p = 53$  steps or 1.325 ms long. Also note that in the  $dq$  reference frame, in general, voltage vectors move the stator flux along curved rather than straight trajectories.

### D. Analysis and Observations

In the following, details about the individual control laws in Fig. 4 are provided. The control law in Fig. 4(a) is based on the assumptions and settings stated in Sect. V-A. The switching losses are minimized. The current switch position is  $\mathbf{u}(k-1) = [-1 \ 0 \ -1]^T$ , while in Fig. 4(d) it is the zero vector  $\mathbf{u}(k-1) = [0 \ 0 \ 0]^T$ .

The resulting regions have clearly defined borders, forming distinctive areas in the state-space, in which the same control input (switch position) is used. When the stator flux vector at time-step  $k$  is within the target window, switching is not required and thus avoided, as exemplified by the almost vertical trajectory in Fig. 4(a). This characteristic will be explained in more detail in Sect. V-E. As a result, within the target window, the control law heavily depends on  $\mathbf{u}(k-1)$ , since this largely determines the switching losses and thus the overall cost.

The controller predicts when the target window will be violated and aims to switch such that any violation is avoided. As an example for this, consider in Fig. 4(a) the lower edge of the target window, which refers to the lower torque bound. Here, switching is performed already when the stator flux is one sampling interval away from the lower torque bound. This time-interval translates to different distances in the state-space, depending on the velocity of the voltage vector relative to the  $dq$  frame. This can be observed when comparing Figs. 4(a) and 4(d) with each other. The voltage vector in Fig. 4(d) roughly points in the same direction, but its velocity is significantly higher. As a result, the band around the lower torque bound, in which switching is performed, is accordingly larger.

When the stator flux vector significantly violates the target window, however, the control laws tend to become similar<sup>2</sup>, irrespective of  $\mathbf{u}(k-1)$ . This can be seen when comparing Figs. 4(a) and 4(d), which only differ with respect to  $\mathbf{u}(k-1)$ . The reason for this is that well outside of the bounds, the

<sup>2</sup>To be precise, the differential mode of the voltage vectors becomes similar. As an example for this, consider in Fig. 4(d) the region with  $\mathbf{u}^*(k) = [0 \ 1 \ 0]^T$  that corresponds in Fig. 4(a) to the region with  $\mathbf{u}^*(k) = [-1 \ 0 \ -1]^T$ . The voltage vectors have the same differential mode voltage, but a different common mode.

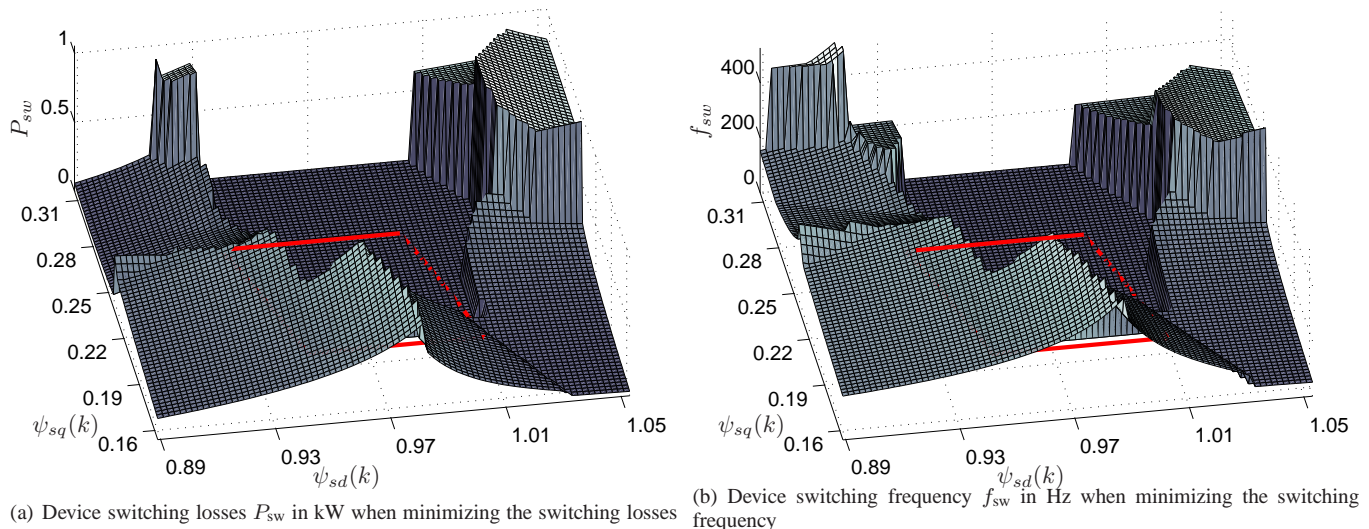


Fig. 5: Predicted switching effort, discounted over the prediction horizon, as a function of the state vector  $\mathbf{x}(k)$  for the current inverter switch position  $\mathbf{u}(k-1) = [-1 \ 0 \ -1]^T$ . The target window is indicated by straight (red) lines. The two figures relate to Figs. 4(a) and 4(b), respectively

bound violation term  $J_{\text{bnd}}$ , which is independent of  $\mathbf{u}(k-1)$ , dominates in the objective function over the switching effort term  $J_{\text{sw}}$ . Moreover, the second constraint in (5d) ensures that only voltage vectors are considered that move the stator flux vector closer to the target window.

When minimizing the switching frequency instead of the switching losses, only minor alterations in the resulting control law result, as shown in Fig. 4(b). Differences arise mostly with regard to the common mode of the voltage vectors, as can be seen in the upper left corner of the figure. When a switching transition from  $\mathbf{u}(k-1) = [-1 \ 0 \ -1]^T$  to a zero vector is required, two options exist, namely  $\mathbf{u}(k) = [-1 \ -1 \ -1]^T$  and  $\mathbf{u}(k) = [0 \ 0 \ 0]^T$ . The first option involves only one switching transition, which is preferable when minimizing the switching frequency. The second option involves two switching transitions with—in this particular case—very small currents in the corresponding phases. Therefore, when minimizing the switching losses, it is advantageous to switch twice, at least in this particular example.

These differences are also reflected in Fig. 5, which shows the predicted switching efforts for the two control laws discussed above. The predicted switching losses in kW are obtained by dividing  $J_P$  by  $1000 T_s$ . A subsequent division by 12 yields the average switching losses per semiconductor device<sup>3</sup>, which are depicted in Fig. 5(a). The device switching frequency is obtained accordingly.

It can be seen that the surfaces of the switching efforts are smooth within the regions. When moving from one region to a neighboring one, the transition is smooth, if both control laws meet the constraint (5d) at the intersection. As an example, consider the regions with the control inputs  $\mathbf{u}^*(k) = [0 \ 1 \ -1]^T$  and  $\mathbf{u}^*(k) = [-1 \ 1 \ -1]^T$ . If, however, one of the control inputs ceases to meet the constraint (5d), then the switching

effort at the transition changes in a step-wise fashion, when moving from one region to a neighboring one. This can be seen at the boundary between the regions with  $\mathbf{u}^*(k) = [-1 \ 0 \ -1]^T$  and  $\mathbf{u}^*(k) = [0 \ 1 \ -1]^T$ . When moving from the first region towards the second one, the control input ceases to meet the constraint, triggering a switching transition and a step-wise change in the switching effort.

Next, consider the control law depicted in Fig. 4(c), which is obtained by setting the weight  $q$  to zero. As a result, only the switching losses are penalized, but no incentive is provided to move the stator flux vector quickly back into the target window. This greatly enlarges the region, in which the previously applied control input is maintained, i.e.  $\mathbf{u}^*(k) = \mathbf{u}(k-1)$ . In this region, as exemplified for the two predicted stator flux trajectories shown in Fig. 4(c), the degree of the bound violation decreases at every time-step. The second constraint in (5d) is thus met, but the convergence rate is slow for the right trajectory. Note that this trajectory terminates when the lower torque bound and hence the constraint (5d) is about to be violated.

Fig. 4(e) shows the control law when lowering the speed operating point to  $\omega_r = 0.1$ . The stator flux trajectories are now effectively straight lines and the zero voltage vector leads to a very slow stator flux movement relative to the  $dq$  reference frame.

So far, we have investigated control laws only for the case where the rotor flux angle is  $\varphi(k) = 0^\circ$ . Fig. 4(f) shows the control law for  $\varphi(k) = 30^\circ$  at nominal speed. When compared to the case  $\varphi(k) = 0^\circ$  shown in Fig. 4(a), the voltage vectors are rotated by  $30^\circ$  and the regions are deformed accordingly.

### E. Visualization of the Control Law Derivation

Additional insight in the derivation of the state-feedback control law is provided hereafter. For this, consider in Fig. 4(a) the control law along the (not shown) line given by  $\psi_{sd} \in$

<sup>3</sup>Recall that an NPC inverter is used with 12 IGBTs.

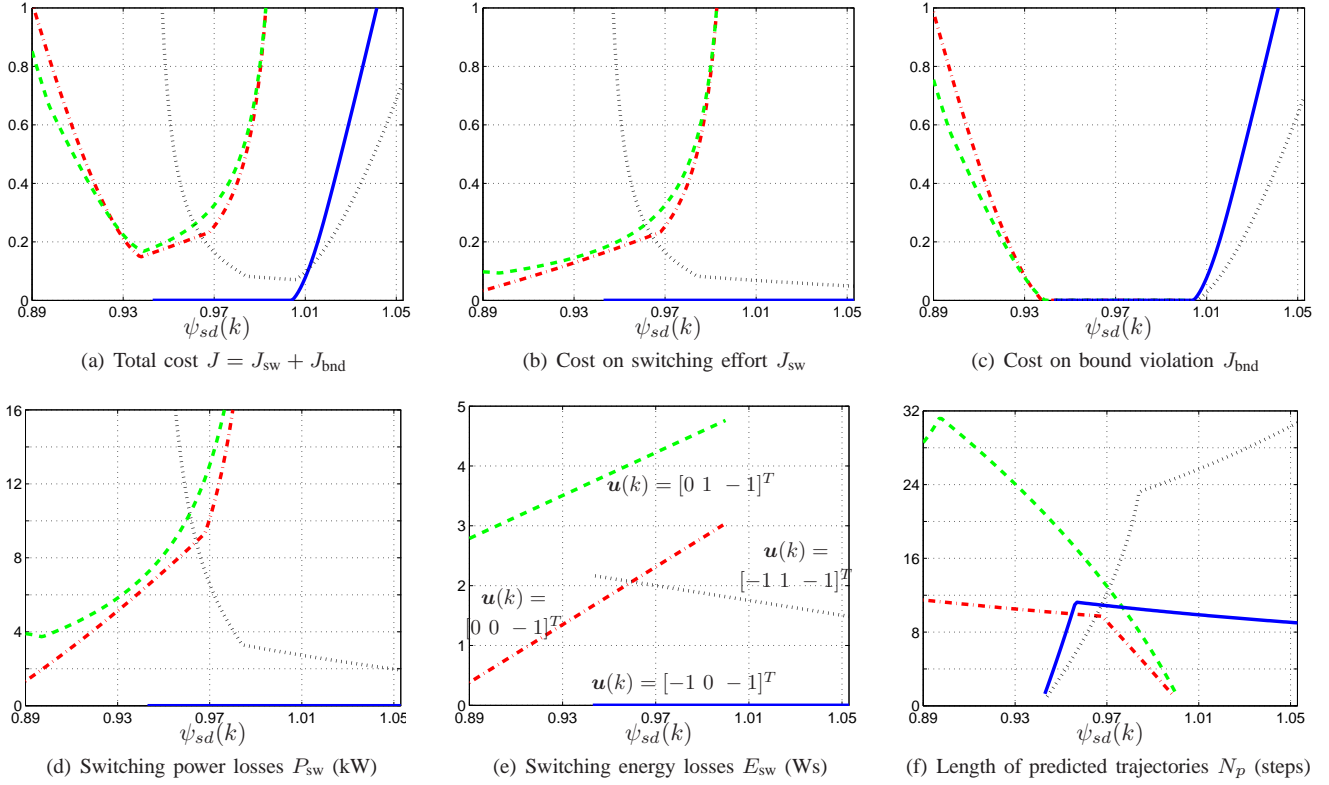


Fig. 6: Visualization of the control law derivation along the line  $\psi_{sd} \in [0.89, 1.054]$  and  $\psi_{sq} = 0.235$  in Fig. 4(a). Four out of the 12 possible switch positions are considered: straight (blue) lines refer to keeping the current switch position, i.e.  $\mathbf{u}(k) = \mathbf{u}(k-1) = [-1 \ 0 \ -1]^T$ , dash-dotted (red) lines imply switching phase  $a$ , i.e.  $\mathbf{u}(k) = [0 \ 0 \ -1]^T$ , dotted (black) lines refer to switching phase  $b$ , i.e.  $\mathbf{u}(k) = [-1 \ 1 \ -1]^T$ , while dashed (green) lines relate to the case in which phases  $a$  and  $b$  are switched, i.e.  $\mathbf{u}(k) = [0 \ 1 \ -1]^T$

$[0.89, 1.054]$  and  $\psi_{sq} = 0.235$ , which corresponds to the torque reference. This line is equivalent to a one-dimensional slice through the state-space  $\mathcal{X}$ . As previously, the current switch position is  $\mathbf{u}(k-1) = [-1 \ 0 \ -1]^T$ , from which transitions to 11 different switch positions are possible, in accordance with the constraint (5e). In Fig. 6, we consider only four options—keeping the current switch position and switching to three new ones. For some state vectors, certain options are not possible, e.g. keeping the current switch position for  $\psi_{sd} < 0.94$  would violate the constraint (5d).

Fig. 6(f) shows the lengths of the predicted stator flux trajectories. Due to the rotation of the reference frame, these lines are slightly curved, but they also exhibit distinctive changes in their slopes. Slope changes result, when the bound, at which the trajectory terminates, changes. Below  $\psi_{sd} < 0.955$ , the straight (blue) line terminates at the lower flux bound, while above this threshold it terminates at the lower torque bound, see also Fig. 4(a).

The switching energy losses in Ws depend on the commutated stator current, which in turn is a linear combination of the stator and rotor flux vectors. The switching energy losses thus depend linearly on the stator flux components. This is confirmed by the distinctively straight lines in Fig. 6(e).

The cost on the switching effort  $J_{sw}$  in Fig. 6(b) is obtained by dividing the switching energy losses by the trajectory

lengths, as explained earlier. As a result, these costs are—similar to the trajectory lengths—slightly curved lines with discontinuities. The switching power losses in Fig. 6(d) are obtained by scaling Fig. 6(b), as described in the previous section.

The cost on the bound violation  $J_{bnd}$  is zero, for as long as the stator flux trajectory remains with the target window. This is the case when the initial state of the stator flux is within the window, as shown in Fig. 6(c). As the starting point of the stator flux trajectory moves away from the target window, the cost on the bound violation increases in an approximately quadratic fashion, due to the quadratic formulation used in (10). The slopes differ between the various switch positions, according to the predicted rms violation of the bounds. For  $\psi_{sd} > 1$ , for example, the switch position  $\mathbf{u}(k-1) = [-1 \ 1 \ -1]^T$  brings the stator flux vector significantly faster back into the target window than  $\mathbf{u}(k-1) = [-1 \ 0 \ -1]^T$  does. This is obvious from Fig. 4(a) and is reflected in Fig. 6(c), in that the former switch position entails a lower penalty on the bound violation.

The total cost  $J$  in Fig. 6(a) is the sum of the costs on the switching effort and on the bound violation, which are shown in Figs. 6(b) and 6(c), respectively. By minimizing the total cost, the optimal control input  $\mathbf{u}^*(k)$  is derived. For  $\psi_{sd} < 0.94$ ,  $\mathbf{u}(k-1) = [0 \ 0 \ -1]^T$  and  $\mathbf{u}(k-1) = [0 \ 1 \ -1]^T$  yield

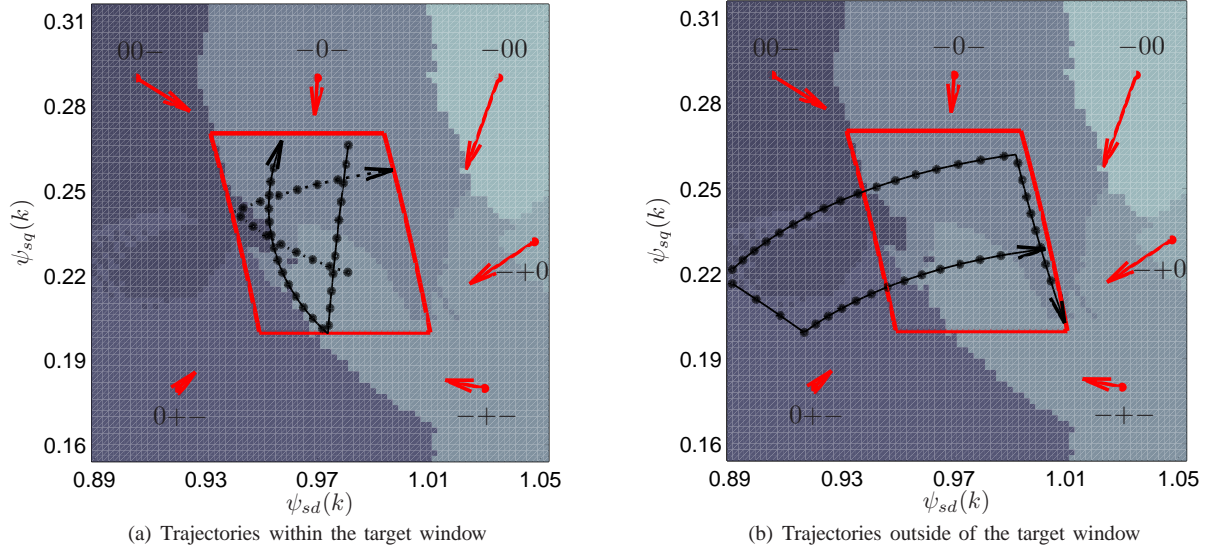


Fig. 7: State-feedback control law for the switching horizon 'SESE' and the inverter switch position  $\mathbf{u}(k-1) = [-1 \ 0 \ -1]^T$ . This figure corresponds to Fig. 4(a) with the switching horizon 'SE'

similar costs. The first switch position incurs a lower switching effort, but tends to be slower in bringing the stator flux vector back into the target window. Therefore, in the interval  $0.92 < \psi_{sd} < 0.94$ , the former is chosen as the optimal control input  $\mathbf{u}^*(k)$ , while for  $\psi_{sd} < 0.92$  the latter is optimal. Within the target window and when slightly violating the upper flux bound, i.e. for  $0.94 < \psi_{sd} < 1$ , it is optimal to not switch, i.e. to use  $\mathbf{u}^*(k) = \mathbf{u}(k-1)$ . For significant violations of the upper flux bound, i.e. for  $\psi_{sd} > 1$ ,  $\mathbf{u}^*(k) = [-1 \ 1 \ -1]^T$  is optimal.

#### F. Analysis for Longer Switching Horizons

So far, the analysis has focused on the switching horizon 'SE'. In this section, longer switching horizons are considered, using 'SESE' as an illustrative example. The same assumptions as previously are used, as summarized in Sect. V-A. Specifically, the switching losses are minimized, the previously applied switch position is  $\mathbf{u}(k-1) = [-1 \ 0 \ -1]^T$ , and the rotor's angular position is  $\varphi(k) = 0^\circ$ .

Using the same algorithm as before to compute the state-feedback control law, the latter is shown in Fig. 7. As previously, several predicted stator flux trajectories are shown as (black) lines with every second sampling instant being indicated by a small circle. Three features distinguish the control law with the switching horizon 'SESE' from the one with 'SE'.

First, switching is scheduled to be performed twice within the prediction horizon, namely at the current time-step  $k$  and again when a bound is predicted to be hit. As a result, two different switch positions are used within the prediction horizon, leading to distinctive vertices in the predicted stator flux trajectories. The control law refers to the first switch position, i.e. to the optimal switch position at time-step  $k$ ,  $\mathbf{u}^*(k)$ . The second, predicted switch position, say  $\mathbf{u}(\ell)$ ,  $\ell > k$ , cannot be directly observed from the control map in Fig. 7. It

can be reconstructed, though, from the direction and velocity of the predicted stator flux trajectory. In general,  $\mathbf{u}(\ell)$  does not coincide with the switch position  $\mathbf{u}^*(k)$  of the region in which the second switching is predicted to occur. As an example, consider the dotted predicted trajectory in Fig. 7(a) and its switching transition at the lower flux bound. The control law associated with the region in which this transition is predicted to occur is  $\mathbf{u}^*(k) = [0 \ 0 \ -1]^T$ , while the second switch position is  $\mathbf{u}(\ell) = [0 \ 1 \ -1]^T$ .

Second, switching is also performed well within the target window, as can be seen in Fig. 7(a). Consider the predicted trajectory with the straight downward-pointing line, for which switching is postponed until the lower torque bound is about to be hit. When moving towards this bound, the number of steps, over which the switching effort can be depreciated, gets smaller and smaller, up to the point, where switching preemptively becomes cheaper than further delaying the switching transition. As a result, the region with the control input  $\mathbf{u}^*(k) = [-1 \ 1 \ -1]^T$  is extended well into the target window. This is exemplified by the dotted trajectory. Therefore, when optimizing over multiple switching transitions, it may be beneficial to switch preemptively.

Third, some regions may not have well-defined boundaries, as can be observed in Fig. 7(b) between the regions with  $\mathbf{u}^*(k) = [0 \ 0 \ -1]^T$  and  $\mathbf{u}^*(k) = [0 \ 1 \ -1]^T$ . Two example trajectories are shown, which start from very similar stator flux positions and provide—despite their different switching sequences—very similar overall costs. By perturbing  $\psi_s(k)$  slightly, one or the other switching sequence is selected. This phenomenon results from the fact that MPDTC operates in the discrete time-domain and that the trajectory length is a natural—rather than a real—number. It is obvious that the length of the upper trajectory is very sensitive to small perturbations in  $\psi_s(k)$ —shifting  $\psi_s(k)$  slightly along the  $d$ -

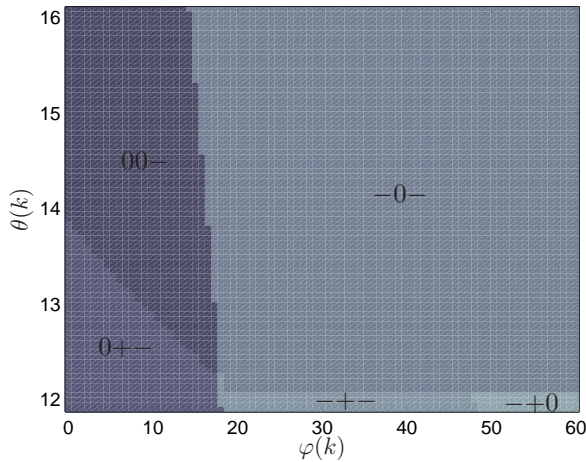


Fig. 8: State-feedback control law along the lower flux bound of the target window for  $\mathbf{u}(k-1) = [-1 \ 0 \ -1]^T$ , where  $\varphi(k)$  represents the angular position of the rotor flux vector and  $\theta(k)$  the (load) angle between the stator and rotor flux vectors. Both angles are given in degrees. The switching horizon 'SE' is used

axis has a major influence on the length of the downward-pointing second part of the trajectory. Reducing the length of the sampling interval mitigates this issue. It is important to point out that both trajectories effectively have the same cost and thus provide the same performance, making the choice between the two irrelevant. In order to avoid switching repeatedly between one strategy and another, it is important that MPDTC adheres to a strategy once selected. This is typically achieved by re-evaluating the control input only once a bound of the target window is about to be violated.

## VI. CONTROL LAW ALONG AN EDGE OF THE TARGET WINDOW

We have seen in Sect. V-D that during steady-state operation, when the stator flux vector is kept within the target window and the switching horizon 'SE' is used, switching is performed effectively only along the edges of the target window.

To gain insight into the dependency of the control law when varying the rotor flux angle, one can compute the control law for different angular positions of the rotor flux vector,  $\varphi(k)$ , as exemplified in Fig. 4(f). An alternative approach is to compute the control law over a two-dimensional space, spanned by the rotor angle and the position along one of the edges of the target window, separately for each of the four edges. The lower flux bound, for example, can be parameterized in polar coordinates using the amplitude  $\Psi_s = \psi_{s,\min}$  and the load angle  $\theta(k)$ , which has previously been defined as the angle between the two flux vectors. In summary, for the lower flux bound, the control law can be derived as a function of the rotor flux angle  $\varphi(k)$  and the load angle  $\theta(k)$ .

The result is shown in Fig. 8, with the angles given in degrees. As expected, the control law for  $\varphi = 0^\circ$  in Fig. 8 is identical to the one in Fig. 4(a) along the lower flux bound (left edge) of the target window. The same holds true for  $\varphi = 30^\circ$  and Fig. 4(f). Due to symmetry properties, it suffices

to compute the control law over an angle span of  $60^\circ$  for  $\varphi$  to fully characterize the controller. The switching effort can also be plotted, similar to Fig. 5.

## VII. CONCLUSIONS

Unlike field oriented and direct torque control, the control law is not directly available in model predictive control (MPC), including model predictive direct torque control (MPDTC). This paper showed a straightforward method to compute the state-feedback control law and—by analyzing and interpreting it—provided new insight into MPDTC.

The derivation and visualization of the control law is paramount during the design process of the controller, since it enables one to analyze and understand the controller's choices, to assess the impact different objective functions have on the closed-loop behavior, to understand the impact of switching constraints, and to evaluate the influence of phenomena such as model uncertainties, observer noise and unaccounted for dc-link voltage fluctuations. Along with plotting the predicted trajectories, the availability of this method constitutes one of the main advantages of MPC over classic control methods, for which the design and tuning process is usually restricted to running closed-loop simulations, and trial and error iterations.

Furthermore, with this tool at ones disposal, the following tasks are envisioned to be achieved in the near future: stability analysis, feasibility analysis, reduction of the computational effort, derivation of switching heuristics and a further improvement of the closed-loop performance. This tool can be used equally well for other predictive drive control concepts, such as one-step predictive control [13], model predictive direct current control (MPDCC) [26], [27], model predictive direct power control [28] and model predictive direct balancing control [29]. It is also straightforward to address multi-level inverter topologies and to include the neutral point potential in the considerations. Since its inception, the derivation of the state-feedback control as described in this paper has proven to be instrumental in analyzing and improving MPDTC. This includes the stability proof for MPDCC in [30].

## ACKNOWLEDGMENT

A research grant from ABB Corporate Research, Baden-Dättwil, Switzerland is gratefully acknowledged by the author.

## REFERENCES

- [1] T. Geyer. *Low Complexity Model Predictive Control in Power Electronics and Power Systems*. PhD thesis, Autom. Control Lab. ETH Zurich, 2005.
- [2] T. Geyer, G. Papafotiou, and M. Morari. Model predictive direct torque control—Part I: Concept, algorithm and analysis. *IEEE Trans. Ind. Electron.*, 56(6):1894–1905, Jun. 2009.
- [3] G. Papafotiou, J. Kley, K. G. Papadopoulos, P. Bohren, and M. Morari. Model predictive direct torque control—Part II: Implementation and experimental evaluation. *IEEE Trans. Ind. Electron.*, 56(6):1906–1915, Jun. 2009.
- [4] T. Geyer. Generalized model predictive direct torque control: Long prediction horizons and minimization of switching losses. In *Proc. IEEE Conf. Decis. Control*, pages 6799–6804, Shanghai, China, Dec. 2009.
- [5] C. E. Garcia, D. M. Prett, and M. Morari. Model predictive control: Theory and practice—A survey. *Automatica*, 25(3):335–348, Mar. 1989.

- [6] J. B. Rawlings and D. Q. Mayne. *Model predictive control: Theory and design*. Nob Hill Publ., Madison, WI, USA, 2009.
- [7] K. H. J. Chong and R.-D. Klug. High power medium voltage drives. In *Proc. IEEE Int. Conf. Power Syst. Technol.*, pages 658–664, Singapore, Nov. 2004.
- [8] I. Takahashi and T. Noguchi. A new quick response and high efficiency control strategy for the induction motor. *IEEE Trans. Ind. Appl.*, 22(2):820–827, Sep./Oct. 1986.
- [9] F. Blaschke. A new method for the structural decoupling of ac induction machines. In *IFAC Symp.*, pages 1–15, Oct. 1971.
- [10] T. Geyer. A comparison of control and modulation schemes for medium-voltage drives: emerging predictive control concepts versus PWM-based schemes. *IEEE Trans. Ind. Appl.*, 47(3):1380–1389, May/Jun. 2011.
- [11] T. Geyer and G. Papafotiou. Model predictive direct torque control of a variable speed drive with a five-level inverter. In *Proc. IEEE Ind. Electron. Soc. Annu. Conf.*, pages 1203–1208, Porto, Portugal, Nov. 2009.
- [12] T. Geyer and S. Mastellone. Model predictive direct torque control of a five-level ANPC converter drive system. *IEEE Trans. Ind. Appl.*, 48(5):1565–1575, Sep./Oct. 2012.
- [13] R. Vargas, P. Cortés, U. Ammann, J. Rodríguez, and J. Pontt. Predictive control of a three-phase neutral-point-clamped inverter. *IEEE Trans. Ind. Electron.*, 54(5):2697–2705, Oct. 2007.
- [14] F. Borrelli, M. Baotić, A. Bemporad, and M. Morari. Dynamic programming for constrained optimal control of discrete-time linear hybrid systems. *Automatica*, 41(10):1709–1721, Oct. 2005.
- [15] M. Kvasnica, P. Grieder, M. Baotić, and M. Morari. Multi parametric toolbox (MPT). In R. Alur and G. Pappas, editors, *Hybrid Syst.: Comput. and Control*, volume 2993 of *LNCS*, pages 448–462. Springer, 2004. <http://control.ee.ethz.ch/~mpt>.
- [16] A. Bemporad and M. Morari. Control of systems integrating logic, dynamics and constraints. *Automatica*, 35(3):407–427, March 1999.
- [17] G. Papafotiou, T. Geyer, and M. Morari. A hybrid model predictive control approach to the direct torque control problem of induction motors (invited paper). *Int. J. of Robust Nonlinear Control*, 17(17):1572–1589, Nov. 2007.
- [18] T. Geyer, G. Papafotiou, R. Frasca, and M. Morari. Constrained optimal control of the step-down dc-dc converter. *IEEE Trans. Power Electron.*, 23(5):2454–2464, Sep. 2008.
- [19] T. Geyer and G. Papafotiou. Direct torque control for induction motor drives: A model predictive control approach based on feasibility. In M. Morari and L. Thiele, editors, *Hybrid Syst.: Comput. and Control*, volume 3414 of *LNCS*, pages 274–290. Springer, Mar. 2005.
- [20] A. Linder and R. Kennel. Model predictive control for electrical drives. In *Proc. IEEE Power Electron. Spec. Conf.*, pages 1793–1799, Recife, Brasil, 2005.
- [21] S. Mastellone, G. Papafotiou, and E. Liakos. Model predictive direct torque control for MV drives with LC filters. In *Proc. Eur. Power Electron. Conf.*, pages 1–10, Barcelona, Spain, Sep. 2009.
- [22] P. C. Krause, O. Wasynczuk, and S. D. Sudhoff. *Analysis of Electric Machinery and Drive Systems*. Intersci. Publ. John Wiley & Sons Inc., 2nd edition, 2002.
- [23] Y. Zeinaly, T. Geyer, and B. Egardt. Trajectory extension methods for model predictive direct torque control. In *Proc. App. Power Electron. Conf. and Expo.*, pages 1667–1674, Fort Worth, TX, USA, Mar. 2011.
- [24] T. Geyer. Computationally efficient model predictive direct torque control. *IEEE Trans. Power Electron.*, 26(10):2804–2816, Oct. 2011.
- [25] Th. Burtcher and T. Geyer. Deadlock avoidance in model predictive direct torque control. In *Proc. IEEE Energy Convers. Congr. Expo.*, Raleigh, NC, USA, Sep. 2012.
- [26] J. C. Ramirez Martinez, R. M. Kennel, and T. Geyer. Model predictive direct current control. In *Proc. IEEE Int. Conf. Ind. Technol.*, pages 1808–1813, Viña del Mar, Chile, Mar. 2010.
- [27] T. Geyer. Model predictive direct current control: formulation of the stator current bounds and the concept of the switching horizon. *IEEE Ind. Appl. Mag.*, 18(2):47–59, Mar./Apr. 2012.
- [28] T. Geyer, J. Scoltock, and U. Madawala. Model predictive direct power control for grid-connected converters. In *Proc. IEEE Ind. Electron. Soc. Annu. Conf.*, Melbourne, Australia, Nov. 2011.
- [29] F. Kieferndorf, P. Karamanakos, Ph. Bader, N. Oikonomou, and T. Geyer. Model predictive control of the internal voltages of a five-level active neutral point clamped converter. In *Proc. IEEE Energy Convers. Congr. Expo.*, Raleigh, NC, USA, Sep. 2012.
- [30] T. Geyer, R. P. Aguilera, and D. E. Quevedo. On the stability and robustness of model predictive direct current control. In *Proc. IEEE Int. Conf. Ind. Technol.*, Cape Town, South Africa, Feb. 2013.